2022

Unique Features of Alarmone Metabolism in *Clostridioides difficile*

Asia Poudel
Old Dominion University, apoud002@odu.edu

Astha Pokhrel
Old Dominion University, apokhrel@odu.edu

Adenrele Oludiran
Old Dominion University, aolud001@odu.edu

Estevan J. Coronado
Old Dominion University

Kwincy Alleyne
Old Dominion University, kalleyne@odu.edu

See next page for additional authors

Original Publication Citation

Poudel, A., Pokhrel, A., Oludiran, A., Coronado, E. J., Alleyne, K., Gilfus, M. M., Gurung, R. K., Adhikari, S. B., Purcell, E. B., & Federle, M. J. (2022). Unique features of alarmone metabolism in *Clostridioides difficile*. *Journal of Bacteriology*, *204*(4), 1-18, Article e00575-21. https://doi.org/10.1128/jb.00575-21

AMERICAN SOCIETY FOR MICROBIOLOGY | Journal of Bacteriology®

RESEARCH ARTICLES

Unique Features of Alarmone Metabolism in *Clostridioides difficile*

Asia Poudel,[a] Astha Pokhrel,[a] Adenrele Oludiran,[a] Estevan J. Coronado,[a] Kwincy Alleyne,[a] Marrett M. Gilfus,[a] Raj K. Gurung,[a] Surya B. Adhikari,[a] Erin B. Purcell[a]

[a]Old Dominion University, Department of Chemistry and Biochemistry, Norfolk, Virginia, USA

ABSTRACT The "magic spot" alarmones (pp)pGpp, previously implicated in *Clostridioides difficile* antibiotic survival, are synthesized by the RelA-SpoT homolog (RSH) of *C. difficile* (RSH_{Cd}) and $RelQ_{Cd}$. These enzymes are transcriptionally activated by diverse environmental stresses. RSH_{Cd} has previously been reported to synthesize ppGpp, but in this study, we found that both clostridial enzymes exclusively synthesize pGpp. While direct synthesis of pGpp from a GMP substrate, and (p)ppGpp hydrolysis into pGpp by NUDIX hydrolases, have previously been reported, there is no precedent for a bacterium synthesizing pGpp exclusively. Hydrolysis of the 5′ phosphate or pyrophosphate from GDP or GTP substrates is necessary for activity by the clostridial enzymes, neither of which can utilize GMP as a substrate. Both enzymes are remarkably insensitive to the size of their metal ion cofactor, tolerating a broad array of metals that do not allow activity in (pp)pGpp synthetases from other organisms. It is clear that while *C. difficile* utilizes alarmone signaling, its mechanisms of alarmone synthesis are not directly homologous to those in more completely characterized organisms.

IMPORTANCE Despite the role of the stringent response in antibiotic survival and recurrent infections, it has been a challenging target for antibacterial therapies because it is so ubiquitous. This is an especially relevant consideration for the treatment of *Clostridioides difficile* infection (CDI), as exposure to broad-spectrum antibiotics that harm commensal microbes is a major risk factor for CDI. Here, we report that both of the alarmone synthetase enzymes that mediate the stringent response in this organism employ a unique mechanism that requires the hydrolysis of two phosphate bonds and synthesize the triphosphate alarmone pGpp exclusively. Inhibitors targeted against these noncanonical synthetases have the potential to be highly specific and minimize detrimental effects to stringent response pathways in commensal microbes.

KEYWORDS *Clostridioides difficile*, (p)ppGpp, (pp)pGpp, alarmone, stringent response, small alarm synthetase

Clostridioides (formerly *Clostridium*) *difficile* is a Gram-positive, spore-forming anaerobic gastrointestinal pathogen that causes *Clostridioides difficile* infection (CDI), which is multidrug resistant and has a high rate of recurrence (1). *C. difficile* is transmitted to susceptible hosts via fecal-oral transmission (2). Once spores are ingested, they survive the acidic pH of the stomach and travel through the intestine, where they interact with primary bile salts and amino acids that facilitate their germination into vegetative cells that secrete protein toxins which cause symptomatic disease (3). The most significant risk factor for CDI development is alteration of the normal gut microflora after exposure to broad-spectrum antibiotics (1, 4).

C. difficile must navigate a dynamic and hostile environment to establish symptomatic infection. The proliferation of vegetative cells in the gut environment is impacted by several factors, including the host immune response, oxygen levels, nutrient limitation, secondary

Editor Michael J. Federle, University of Illinois at Chicago

Address correspondence to Erin B. Purcell, epurcell@odu.edu.

The authors declare no conflict of interest.

Received 12 November 2021
Accepted 1 February 2022
Published 7 March 2022

bile acids, short-chain fatty acids, competing gut microflora, and various pHs throughout the gastrointestinal tract (5–8). The immune response to gastrointestinal infection can include fever of 1 to 4°C, antimicrobial host defense peptides, sequestration of metals to limit their availability, and oxidative stress from reactive oxygen species (ROS) and reactive nitrogen species (RNS) (9–13).

The stringent response (SR) is a stress survival mechanism that enables bacterial cells to quickly adapt to extracellular stress by temporarily halting growth and cell division and inducing transcription of stress survival genes (14, 15). The SR contributes to regulation of bacterial growth, virulence, antimicrobial peptide survival, oxidative stress resistance, antibiotic tolerance, and persistence in diverse bacterial pathogens (16). This process is canonically driven by the accumulation of two intracellular alarmone nucleotides, guanosine pentaphosphate (pppGpp) and guanosine tetraphosphate (ppGpp), collectively known as (p)ppGpp and sometimes referred to as "magic spots" (17). These signaling molecules are metabolized by multidomain bifunctional synthetase/hydrolase enzymes in the long RelA-SpoT homolog (RSH) family and by monofunctional small alarmone synthetase (SAS) and small alarmone hydrolase (SAH) domains (18). Extracellular stresses, including amino acid starvation, alkaline shock, cell wall stress from cell wall-active antibiotics, heat stress, oxidative stress, and acid stress can trigger the SR by modulating the transcription of either RSH or SAS genes (14, 19, 20). Posttranslational regulation of RSH enzymes typically involves protein-protein interactions or binding of uncharged tRNAs, while posttranslational regulation of SAS enzyme seems to depend on allosteric binding of (p)pGpp (21–24). The SAS enzymes also appear to play a stress-independent role in maintaining basal alarmone levels and regulating guanosine homeostasis in *Bacillus subtilis* and *Enterococcus faecalis* (25–27).

Guanosine substrate utilization varies among characterized alarmone synthetases, hinting at different biological roles. We have previously reported that the RSH of *C. difficile* (RSH_{Cd}) binds both GDP and GTP *in vitro* but exclusively utilizes GDP as a phosphoacceptor (28). This is unusual among RSH family enzymes, which utilize both GDP and GTP with various affinities to synthesize ppGpp and pppGpp and typically have higher affinity for GTP in Gram-positive organisms (18, 29–33). In addition, RSH homologs from *B. subtilis* and *Methylorubrum* (formerly *Methylobacterium*) *exotorquens* have recently been reported to synthesize (p)ppApp when incubated with adenosine phosphoacceptors (34, 35). The RelP and RelQ enzymes of *B. subtilis*, *E. faecalis*, and *Staphylococcus aureus* all exhibit greater affinity for GDP than GTP (25, 36, 37). RelZ from *Mycobacterium smegmatis*, which contains an RNase H domain in addition to the SAS, utilizes GMP preferentially (38). RelS from *Corynebacterium glutamicum*, part of a subfamily found only in *Acinetobacter*, has a higher affinity for GTP (39). *C. glutamicum* also contains a RelP homolog, RelP*, which lacks conserved amino acids at its C terminus and has no (pp)pGpp synthetic capacity (39).

Firmicutes species typically encode a single RSH and one or two SASs (18). The highly conserved synthetase domains of both families catalyze the transfer of a pyrophosphate moiety from ATP to 3′-OH of GDP and GTP to produce ppGpp and pppGpp, respectively (17). SAS enzymes from several Gram-positive species were recently discovered to synthesize a third alarmone, pGpp, utilizing GMP as a substrate (25, 39, 40). In addition, NUDIX hydrolases remove 5′ phosphates or pyrophosphates from ppGpp or pppGpp to produce pGpp (25, 38, 40–42). The physiological role of pGpp as a third alarmone is still under investigation. It has been speculated to allow a prolonged SR after the depletion of cytoplasmic GTP and GDP (25, 39). We henceforth refer to the three alarmones collectively as (pp)pGpp where appropriate.

Here, we report that expression of clostridial (pp)pGpp synthetase genes is induced by antibiotic stress and several stresses that mimic those produced by the immune system, including acid and oxidative stress and limited metal ion availability. We further report that the $RelQ_{Cd}$ enzyme utilizes both GDP and GTP as substrates but that the only form of alarmone produced by either the RSH_{Cd} or $RelQ_{Cd}$ enzyme is pGpp. Activity of both enzymes depends upon 5′ β phosphate bond hydrolysis of the GXP substrate. We found that $RelQ_{Cd}$, like RSH_{Cd}, tolerates a remarkable diversity of divalent

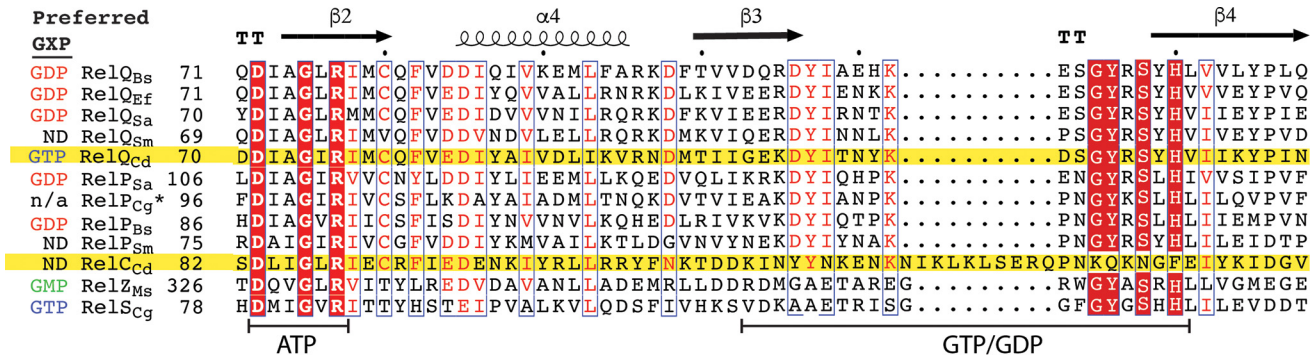

FIG 1 Substrate binding sites of SAS enzymes. The sequences of characterized SAS enzymes from *Bacillus subtilis*, *E. faecalis*, *S. aureus*, *S. mutans*, *C. difficile*, *C. glutamicum*, and *M. smegmatis* are aligned with the crystal structure of *Bacillus subtilis* RelQ (PDB code 5DED). The clostridial sequences RelQ and RelC are highlighted in yellow. β-Strands are shown as arrows, and α-helices are shown as corkscrews. Conserved residues are shown in red, and highly conserved residues are shown in white on a red background. ATP and GDP binding motifs identified in $RelQ_{Bs}$ and $RelP_{Sa}$ are indicated at the bottom. The preferred guanosine nucleotide substrate of enzymes that have been kinetically characterized are shown on the left. "ND" indicates that the substrate preference of an enzyme has not been determined; "n/a" indicates that the enzyme is not active as a (pp)pGpp synthetase. Alignment was generated with ESPript 3 (https://espript.ibcp.fr/ESPript/ESPript/).

metal ion cofactors. The seemingly exclusive production of pGpp is unique to *C. difficile* among previously studied bacteria.

(The thin-layer chromatography [TLC] image in Fig. 4B was previously reported in Appendix D of Astha Pokhrel's doctoral dissertation, "Evaluating the Role of the Stringent Response Mechanism in *Clostridioides difficile* Survival and Pathogenesis" [43].)

RESULTS

***C. difficile* encodes one conserved SAS and one divergent SAS.** We have previously reported that *C. difficile* encodes an RSH family enzyme and the SAS $RelQ_{Cd}$ (CDR20291_0350) and confirmed the enzymatic activity of RSH_{Cd} (CDR20291_2633) (28). In addition to RelQ, *C. difficile* encodes another putative SAS enzyme, CDR20291_1607, which we have named RelC. RelC contains a putative SAS domain and a C-terminal 250-residue region that contains no conserved domain, and its only homologs are in *Firmicutes* species (18). $RelQ_{Cd}$ exhibits high sequence conservation in the ATP and GDP binding motifs identified in crystal structures of RelQ of *B. subtilis* ($RelQ_{Bs}$) and RelP of *S. aureus* ($RelP_{Sa}$) (Fig. 1) (31, 44). RelC has a highly conserved ATP binding motif, but the putative GDP binding motif lacks several conserved residues, including a tyrosine (Y116 in $RelQ_{Bs}$, Y151 in $RelP_{Sa}$, and Q137 in RelC) that stacks with the guanosine base in the GDP substrate and is invariant in SAS and RSH synthetase domains (31, 44). In addition, RelC contains a 10-residue insert within the GDP recognition motif that has no homolog in any characterized SAS (Fig. 1). Initial attempts to express RelC in *Escherichia coli* for purification were unsuccessful, but further experimentation will be necessary to determine whether RelC binds any form of guanosine substrate or serves as a pyrophosphotransferase (Fig. 1).

***C. difficile* induces *rsh* and *relQ* transcription in response to clinically relevant antibiotic stress.** In our earlier work, we utilized an anaerobic fluorescent transcriptional reporter incorporating the oxygen-independent fluorescent flavoprotein phiLOV2.1 to monitor transcription of the clostridial *rsh* and *relQ* genes (28). We observed the increased transcription of these genes upon exposure to sublethal concentrations of clindamycin and metronidazole (28). Antibiotic-induced synthetase gene expression differed between the epidemic strain *C. difficile* R20291 and the laboratory strain *C. difficile* 630Δ*erm* despite the complete conservation of the *relQ* promoter between strains and the nearly complete (except for a single purine substitution) conservation of the *rsh* promoter. The protein sequences of both synthetases and of RelC are completely conserved between the strains (28). In this study, we extended these findings using two other antimicrobials, vancomycin and fidaxomicin, the currently recommended antibiotic treatments for severe or recurring CDI (45, 46). Exponentially growing cells were exposed to

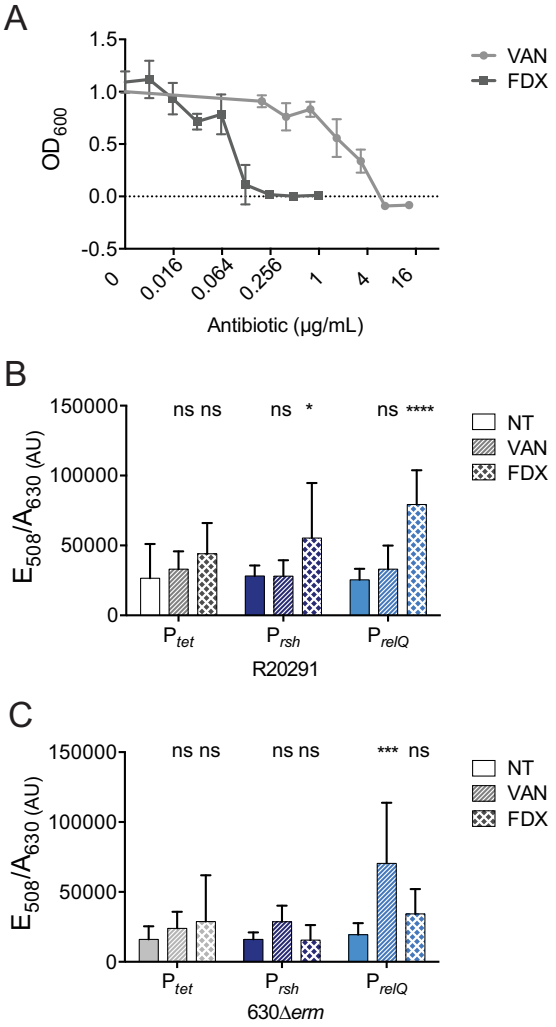

FIG 2 Transcriptional response of (pp)pGpp synthetase genes to antibiotic stress. (A) Overnight growth of R20291 at the indicated concentrations of vancomycin (VAN) and fidaxomicin (FIX). Shown are the means and standard deviations of nine biologically independent samples. (B and C) PhiLOV fluorescence normalized to cell density after 2 h of exposure to 1.7 μg mL^{-1} of vancomycin or 0.067 μg mL^{-1} of fidaxomicin. Shown are the means and standard deviations of at least six biologically independent samples in the R20291 (B) and 630Δ*erm* (C) backgrounds. Conditions with antibiotics were compared to those without (NT) by two-way analysis of variance (ANOVA). ****, $P < 0.0001$; *, $P < 0.05$. ns, not significant.

drug concentrations 0.5× those sufficient to inhibit growth (Fig. 2A; see also Fig. S1 in the supplemental material). In the *C. difficile* R20291 and *C. difficile* 630Δ*erm* strains, promoter activity in the tetracycline-inducible control strain was unaffected by either antibiotic. In *C. difficile* R20291, vancomycin had no effect on transcription from the *rsh* or *relQ* promoter, while fidaxomicin stimulated a 96% increase in P_{rsh} activity and a 3.1-fold increase in P_{relQ} activity (Fig. 2B). In *C. difficile* 630Δ*erm*, the P_{rsh} reporter had no response to either drug, while activity from the P_{relQ} reporter increased 3.6-fold upon exposure to vancomycin (Fig. 2C).

***rsh* and *relQ* transcription during oxidative, heat, and pH stress.** To assess the potential role of (pp)pGpp signaling and the stringent response in *C. difficile* survival of environmental stresses within the host, we monitored *rsh* and *relQ* promoter activity in *C. difficile* R20291 under conditions mimicking potential stressors *in vivo*. Activity from both promoters was indistinguishable after incubation at either 37°C or 41°C, suggesting that even high fever within a mammalian host would not activate transcription of

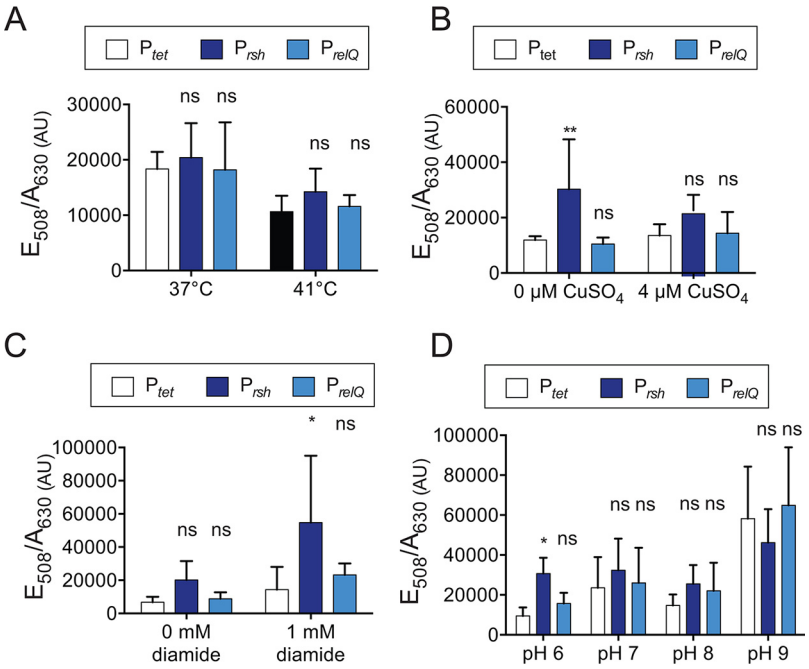

FIG 3 Transcriptional response of (pp)pGpp synthetase genes to environmental stress in R20291. (A) PhiLOV fluorescence normalized to cell density after 30 min of incubation at the indicated temperature. Shown are the means and standard deviations of six biologically independent samples. (B) PhiLOV fluorescence normalized to cell density after 2 h of exposure to the indicated concentration of copper sulfate. Shown are the means and standard deviations of six biologically independent samples. (C) PhiLOV fluorescence normalized to cell density after 3 h of exposure to the indicated concentration of diamide. Shown are the means and standard deviations of three biologically independent samples. (D) PhiLOV fluorescence normalized to cell density 3 h after transfer from unbuffered BHIS to BHIS buffered at the indicated pH with potassium phosphate buffer. Activity from the P_{rsh} and P_{relQ} promoters was compared to that from the P_{tet} promoter under the same condition by two-way ANOVA. *, $P < 0.05$; **, $P < 0.01$.

(pp)pGpp synthetase genes (Fig. 3A). Oxidative stress was mimicked through exposure to copper, a transition metal previously shown to inhibit *C. difficile* growth, and to diamide, an oxidant that mimics oxidative stress in anaerobes by instigating disulfide bonds (47, 48). We have previously shown that 4 μM $CuSO_4$ prevents *C. difficile* growth (47). In this study, we have determined that 1 mM diamide is similarly inhibitory (Fig. S1). Three hours of exposure to copper did not stimulate increased activity from the *rsh* or *relQ* promoter; indeed, *rsh* promoter activity was somewhat decreased after copper treatment (Fig. 3B). Treatment with diamide stimulated a 3.8-fold increase in *rsh* promoter activity but had no effect on the *relQ* promoter (Fig. 3C). While the baseline fluorescence of the P_{tet} reporter strain increased under alkaline conditions, transfer to media buffered at neutral or alkaline pH had no effect on the activity of either clostridial promoter relative to that of the of the P_{tet} reporter (Fig. 3D). However, transfer from unbuffered brain heart infusion medium supplemented with 5% yeast extract (BHIS; initial pH measured at 7.4) to BHIS buffered at pH 6 did stimulate a 3.2-fold increase in P_{rsh} activity (Fig. 3D). Notably, when we measured the pH of spent BHIS after 24 h of *C. difficile* growth, we found that R20291 acidified its growth medium to pH 6. Medium acidification by 630Δ*erm* was less pronounced (Table 1). We have previously shown that *rsh* transcription in *C. difficile* 630Δ*erm* is induced by stationary-phase onset. It is possible that medium acidification, in addition to nutrient depletion, triggers this response.

$RelQ_{Cd}$ is an active (pp)pGpp synthetase. We have previously reported the *in vitro* synthetase activity of RSH_{Cd}, which transfers pyrophosphate to GDP phosphoacceptors exclusively (28). In this study, we confirmed that the putative synthetase RelQ from this

TABLE 1 pHs of fresh and spent BHIS medium[a]

	pH	
***C. difficile* strain**	**Fresh BHIS**	**24-h spent BHIS**
R20291	7.44	6.06
630Δ*erm*	7.44	6.94

[a]pH of growth medium was measured before and 24 h after inoculation with single colonies.

organism is also active *in vitro*, capable of transferring a pyrophosphate moiety from [γ-^{32}P]ATP to a guanosine nucleotide phosphoacceptor (Fig. S2A). Unlike RSH_{Cd}, $RelQ_{Cd}$ activity is concentration dependent and exhibits little to no pyrophosphotransfer activity at concentrations below 0.4 μM (Fig. S2A). This may explain why overexpression of $RelQ_{Cd}$ in *E. coli* does not arrest cell division as we previously observed with RSH_{Cd} overexpression (Fig. S2B) (28). SAS from *B. subtilis*, *S. aureus*, and *E. faecalis* function as tetramers, raising the possibility that $RelQ_{Cd}$ is not expressed in *E. coli* at levels sufficient to allow oligomerization and alarmone synthesis *in vivo* (31, 44, 49).

$RelQ_{Cd}$ utilizes GDP and GTP but synthesizes pGpp exclusively. In order to assess the substrate specificity of $RelQ_{Cd}$, we performed synthesis assays utilizing the monophosphate, diphosphate, and triphosphate forms of both adenosine and guanosine nucleotides as phosphoacceptors. We found that $RelQ_{Cd}$ is incapable of transferring pyrophosphate from ATP to any adenosine nucleotides or to GMP (Fig. 4A). $RelQ_{Cd}$ utilizes both GDP and GTP as phosphoacceptors but synthesizes the same-size product rather than the expected ppGpp and pppGpp, which should migrate differently on a chromatogram due to the additional mass and charge of the pentaphosphate alarmone (Fig. 4A). We performed synthesis assays using the same range of adenosine and guanosine phosphoacceptors with the RelQ enzyme from *Bacillus subtilis*, which is known to utilize GMP, GDP, and GTP *in vitro* in order to synthesize pGpp, ppGpp, and pppGpp, respectively (27, 34). As predicted, $RelQ_{Bs}$ utilized the three guanosine nucleotide substrates to synthesize three differently sized products. Unexpectedly, the single product synthesized by $RelQ_{Cd}$ had the same apparent size and charge as pGpp synthesized by $RelQ_{Bs}$ from ATP and GMP, rather than ppGpp (Fig. 4A). Upon further exploration of guanosine utilization by these enzymes, it was found that RSH_{Cd} utilized GDP to synthesize an apparent pGpp product rather than ppGpp as we had previously reported (28). In this assay, RSH_{Cd} exhibited some trace synthesis of an apparent pGpp product using GTP as a substrate, although the pGpp spot was very faint and could have resulted from GDP contamination in the GTP sample (Fig. 4B). $RelQ_{Bs}$ again utilized mono-, di-, and triphosphate guanosine substrates to synthesize tri-, tetra-, and pentaphosphate products, respectively. $RelQ_{Cd}$ utilized both GDP and GTP as substrates but only synthesized the apparent triphosphate pGpp product. Neither clostridial enzyme utilized GMP as a substrate, and neither synthesized any product other than the apparent triphosphate magic spot pGpp.

To rule out the possibility that the clostridial enzymes synthesize ppGpp or pppGpp and then convert it to pGpp through an intrinsic hydrolysis capability, we incubated $RelQ_{Cd}$ with ppGpp and pppGpp produced by $RelQ_{Bs}$. After an hour of incubation, the exogenously produced magic spots had not been hydrolyzed and no pGpp spot had emerged, suggesting that under the experimental conditions tested, $RelQ_{Cd}$ synthesizes pGpp directly rather than converting ppGpp or pppGpp intermediates (Fig. 4C). This suggests that the clostridial synthetases could hydrolyze 5′ phosphate bonds on their guanosine substrates even as they ligate pyrophosphates to the 3′ hydroxyl groups (Fig. 4D).

Under the conditions studied, $RelQ_{Cd}$ appeared to consume all of the [γ-^{32}P]ATP provided in the presence of GTP but leave more residual ATP in the presence of GDP, suggesting a higher affinity for the triphosphate substrate (Fig. 4A). Kinetic analysis of enzyme activity at multiple concentrations of guanosine substrate yielded calculated

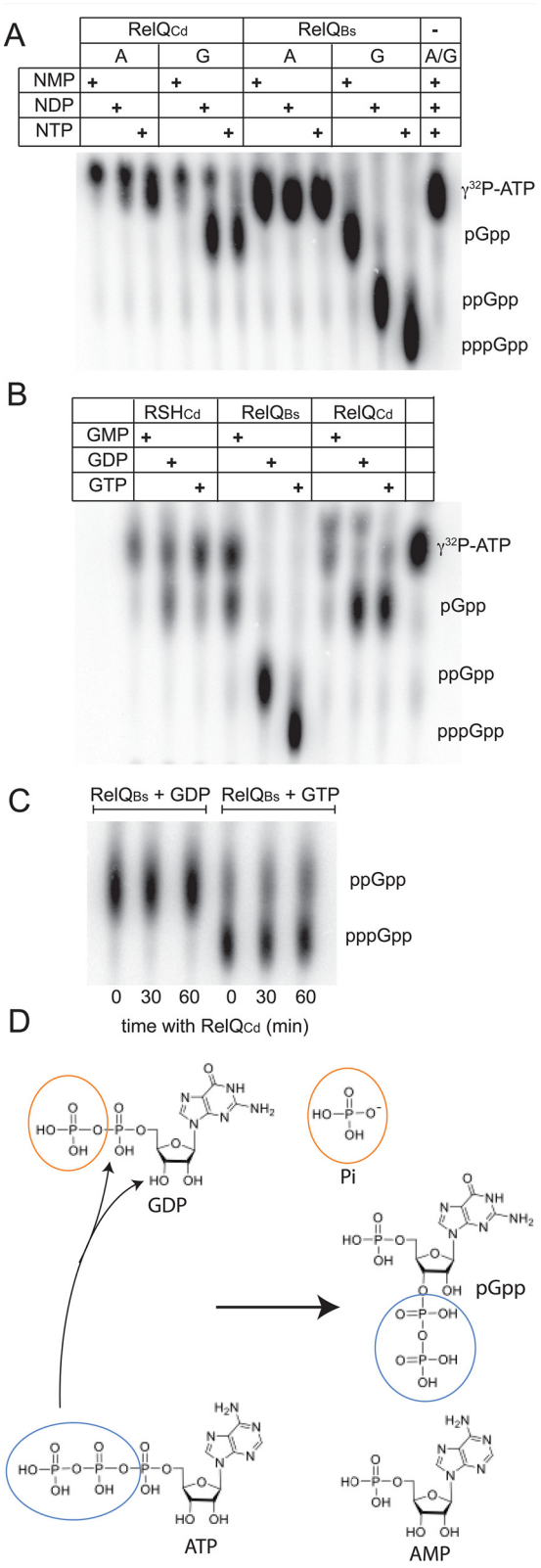

FIG 4 $RelQ_{Cd}$ utilizes GDP and GTP but exclusively synthesizes pGpp. (A) Pyrophosphotransfer after 60 min from [γ-^{32}P]ATP to a 500 μM concentration of the indicated purine nucleotide phosphoacceptors by 2.0 μM $RelQ_{Cd}$ or 3.0 μM $RelQ_{Bs}$. (B) Pyrophosphotransfer after 60 min from [γ-^{32}P]ATP to a 500 μM concentration of the indicated guanosine nucleotide phosphoacceptors by 3.0 μM RSH_{Cd}, 3.0 μM $RelQ_{Bs}$, or 2.0 μM $RelQ_{Cd}$. (C) After $RelQ_{Bs}$ was incubated with GDP or GTP for 60 min, $RelQ_{Cd}$ was added to the

(Continued on next page)

Michaelis constants of 45.4 μM for GTP and 53.6 μM for GDP, consistent with the visual observations (Table 2; Fig. S3). In order to further quantitate the affinity of $RelQ_{Cd}$ for its guanosine substrate, we performed isothermal titration calorimetry. We found that the affinity constant of $RelQ_{Cd}$ for GDP is roughly half that for GTP (Table 2). While the two methods did not produce a consensus for the absolute binding affinity of RelQ for its guanosine substrates, they were consistent in indicating that the enzyme has higher affinity for the triphosphate substrate under the experimental conditions. As RSH_{Cd} has a higher affinity for GDP than GTP *in vitro*, these results suggest that the two synthetases may be differentially active under discrete cellular conditions when either GTP or GDP is more prevalent.

The clostridial magic spot is pGpp. To confirm the identity of the clostridial alarmone product, we investigated the ^{31}P chemical shifts of the clostridial synthetase reactions. When ATP is mixed with GDP or GTP, the resonant peaks of each phosphorus are clearly visible and are consistent with the peaks of the individual nucleotides (Fig. 5C; Fig. S4) (50, 51). The chemical shifts of each of the phosphorus groups are listed in Table S1. The putative triphosphate alarmone pGpp contains a 5′ α phosphate with resonant peak near those in AMP and GMP (Fig. 5A to C). The alarmone also contains a 3′ diphosphate with α and β phosphates whose resonant peaks are very near those of the 5′ α and β phosphates of GDP or the α and γ phosphates of GTP (Fig. 5A, Fig. S4, and Table S1). When ATP and GDP were incubated with $RelQ_{Cd}$, the 5′ α peak of the ATP triphosphate at -10.71 ppm was reduced and a 5′ α monophosphate peak identical to that of the AMP peak at 3.49 ppm appeared at 3.52 ppm. Incubation with RelQ also reduced the ATP β and γ phosphate peaks at -19.16 ppm and -5.58 ppm, consistent with ATP hydrolysis (Fig. 5B, D, and E). The peaks at -10.10 ppm and -6.18 ppm, ascribed to the 5′ α and β phosphates of GDP, were broadened, presumably by overlap with the peaks of the chemically similar 3′ α and β phosphates of pGpp (Fig. 5D and E). A new peak appeared at 4.02, close to but distinct from that of the 5′ α monophosphate peak of GMP at 3.28 ppm, which we ascribe to a 5′ α monophosphate (Fig. 5C and E). In addition, an enormous peak appeared at 2.2 ppm, identical to published values for inorganic phosphate (Fig. 5E, F and H). These results are all consistent with transfer of a pyrophosphate from ATP to the 3′ OH of GDP, accompanied by hydrolysis of the 5′ β phosphate bond of GDP and release of inorganic phosphate.

Similar results were obtained when ATP and GDP were incubated with RSH_{Cd}, confirming that our previous identification of the RSH_{Cd} product as ppGpp was erroneous (Fig. 5D and F). The signal from the α, β, and γ 5′ phosphates of ATP diminished, while a 5′ α monophosphate AMP peak and a 5′ α pGpp peak emerged (Fig. 5F). The α and β phosphate peaks of GDP differentiated into doublet peaks, presumably from interaction with the similar pGpp 3′ α and β phosphates. We attribute the greater loss of ATP peaks and greater differentiation of the guanosine α and β phosphate peaks to greater enzymatic activity by RSH, for which GDP is the preferred substrate, and subsequently less residual ATP and GDP in the reaction mixture.

When ATP and GTP were mixed, the α and γ phosphates of the two triphosphate substrates presented as doublet peaks, while the β phosphates presented as one broad peak (Fig. 5G). When ATP and GTP were incubated with $RelQ_{Cd}$, the 5′ α phosphate peak of pGpp appeared at 4.03 ppm and peaks appeared at -5.83 ppm and -10.39 ppm, consistent with the diphosphate of GDP or pGpp and not present in GTP appear (Fig. 5G and H).

When the enzymes were incubated with guanosine substrates in the absence of ATP, the inorganic phosphate peaks were very small relative to the peaks from the guanosine phosphates, suggesting that either ATP hydrolysis or pyrophosphotransfer

FIG 4 Legend (Continued)
reaction for the indicated time and reaction products were analyzed by TLC. Each of the images shown is representative of at least three experiments. (D) The proposed reaction of pGpp synthesis via pyrophosphate transfer from ATP to the 3′ hydroxyl group of GDP with concurrent phosphate bond hydrolysis and inorganic phosphate release from the 5′ diphosphate of GDP.

TABLE 2 Substrate affinity of $RelQ_{Cd}$ at 37°C[a]

Type of analysis and substrate	K_m (μM^{-1})	K (M^{-1})	ΔH (cal mol^{-1})	ΔS (cal $mol^{-1°C-1}$)
Michaelis-Menten				
GDP	45.4			
GTP	53.6			
Isothermal titration calorimetry				
GDP		2.04E3 ± 2.25E3	−8.18E7 ± 8.21E7	−2.64E5
GTP		4.87E4 ± 3.64E3	−1.639E6 ± 7.412E4	−5.25E3

[a]The binding of $RelQ_{Cd}$ at 0.006 mM to GDP/GTP at 0.060 mM was measured by ITC. The data were fitted to a single-binding-site model. Shown are the values for K_m, K (the equilibrium binding constant), ΔH (the enthalpy change associated with protein binding to the ligand), and ΔS (the entropy change associated with binding). Each value is the average of two repeat experiments, and the standard deviations are shown.

stimulates the phosphorolysis of the guanosine substrate (Fig. S5). No peaks attributable to pGpp emerged, confirming that hydrolysis depends on ATP (Fig. S5).

Clostridial synthetases require phosphorolysis of the guanosine substrate. To confirm that the guanosine substrate is hydrolyzed during clostridial magic spot synthesis, we employed 5′-β-thio-diphosphate (GDPβS), which has a nonhydrolyzable thiol bond between the α and β phosphates, as a phosphoacceptor. Both $RelQ_{Cd}$ and RSH_{Cd} synthesized pGpp when GDP was supplied as a substrate, but neither clostridial enzyme generated any form of magic spot when GDPβS was the substrate (Fig. 6). $RelQ_{Cd}$ did appear to deplete the radioactive ATP substrate in the presence of GDPβS but could not complete phosphotransfer, while RSH_{Cd} displayed no activity at all in the absence of a chemically labile β phosphate bond on the guanosine substrate (Fig. 6). $RelQ_{Bs}$ was able to utilize GDPβS as a phosphoacceptor. The product formed by $RelQ_{Bs}$ using GDPβS was larger than ppGpp formed from GDP since the nonhydrolyzable analog contains three lithium atoms that make the product heavier than ppGpp and closer in apparent size to pppGpp formed from GTP (Fig. 6).

$RelQ_{Cd}$ utilizes diverse metal cofactors and may evade nutritional immunity. *In vitro* analyses of RSH or SAS hydrolysis are typically carried out in the presence of micromolar levels of magnesium (17, 25, 30, 31, 39). RSH from *Methylorubrum extorquens* has previously been reported to utilize cobalt more efficiently than magnesium, although its activity is severely curtailed by manganese, calcium, or nickel cofactors, indicating that the enzyme's metal utilization is highly specific (35). We have previously reported that RSH_{Cd} is capable of utilizing multiple structurally diverse divalent cations as cofactors with little to no loss of efficacy compared to magnesium (28). In this study, we found that $RelQ_{Cd}$ also accepts multiple metal ion cofactors with a broad range of atomic radii, both smaller and larger than magnesium (Fig. 7; Table 3). Pyrophosphotransfer to a GDP substrate was robust under almost every condition studied. GDP utilization was modestly reduced by ferrous iron, the smallest metal ion tested (Fig. 7A; Table 3). $RelQ_{Cd}$ utilization of GTP was more sensitive to metal cofactor identity. GTP utilization was decreased by iron, nickel, and copper, despite the last two being very close in size to magnesium (Fig. 7A; Table 3). Even calcium, which is substantially larger than magnesium, effectively substituted as a cofactor. In contrast, $RelQ_{Bs}$ was much more selective for metal ion cofactors. This enzyme exhibited strong pyrophosphotransferase activity to both GDP and GTP substrates with cobalt, nickel, manganese, or magnesium cofactors but very little activity in the presence of iron, zinc, copper, or calcium (Fig. 7B). $RelQ_{Bs}$ does appear to discriminate on the basis of ionic size, as the acceptable metal substitutions are those closest in size to the conventionally used magnesium (Fig. 7B; Table 3). Nickel ions appear to disfavor the use of GTP relative to GDP by both enzymes despite the fact that nickel is very close in size to magnesium, indicating that size is not the only factor that influences metal ion cofactor specificity.

Because magnesium chloride was present in the protein purification buffer, we considered the possibility that residual magnesium rather than the added divalent cations was responsible for the observed activity. To address this, we performed ^{31}P nuclear magnetic resonance (NMR) in the presence of 5 mM $MgCl_2$ and in the absence of any added metal cations. When magnesium chloride was added to the reactions, incubation of $RelQ_{Cd}$ with

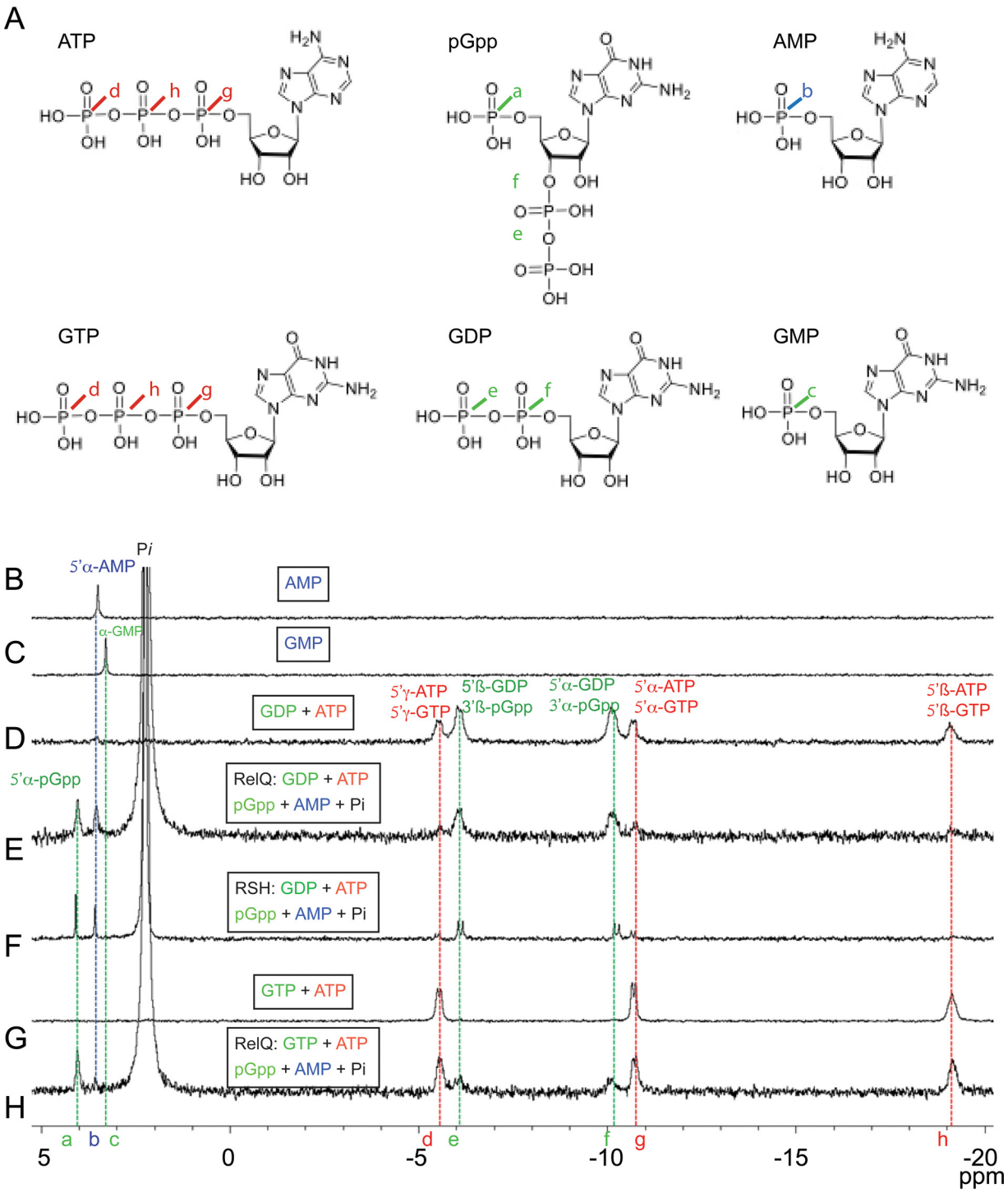

FIG 5 ^{31}P NMR evidence that the clostridial magic spot is pGpp. (A) Structures of nucleotide alarmone substrates and products. Nuclei are labeled according to the peaks assigned to them in the ^{31}P spectra. (B) AMP standard. (C) GMP standard. (D) GDP and ATP standards. (E) GDP and ATP incubated with 2.0 μM $RelQ_{Cd}$ for 40 min. (F) GDP and ATP incubated with 3.0 μM RSH_{Cd} for 60 min. (G) GTP and ATP standards. (H) GTP and ATP incubated with 2.0 μM $RelQ_{Cd}$ for 40 min.

ATP and GDP resulted in the loss of the ATP 5′ β phosphate signal and the concurrent emergence of 5′ α phosphate peaks from pGpp and AMP (Fig. 8A and C). Signal intensity from the ATP 5′ α and 5′ β phosphate peaks was also reduced (Fig. 8A and C). In the absence of supplemental magnesium chloride, incubation of $RelQ_{Cd}$ with ATP and GDP still resulted in the loss of the ATP 5′ β phosphate signal but no gain of the 5′ α phosphate

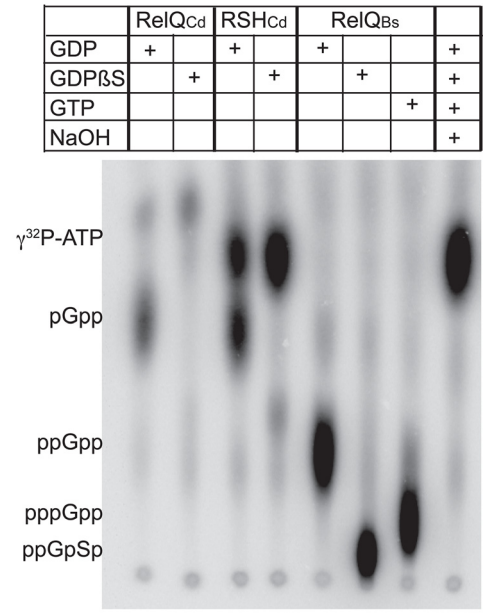

FIG 6 Clostridial synthetases hydrolyze the beta phosphate bond on GXP to synthesize pGpp. Pyrophosphotransfer from [γ-^{32}P]ATP by 2.0 μM $RelQ_{Cd}$, 3.0 μM RSH_{Cd}, or 3.0 μM $RelQ_{Bs}$ to 500 μM GDP, nonhydrolyzable GDPβS, or GTP. The image shown is representative of three experiments.

signal, suggesting that ATP was hydrolyzed but pyrophosphotransfer did not occur under this condition (Fig. 8B). Incubation of RSH_{Cd} with ATP and GDP without magnesium chloride abolished the ATP 5′ β phosphate signal and appeared to result in a small AMP 5′ α phosphate peak, suggesting that residual magnesium was sufficient for RSH_{Cd} ATP hydrolysis to ADP and possibly to AMP (Fig. 8D). Without added metal, RSH_{Cd} did not generate any 5′ α phosphate signal from pGpp, which was robust when RSH_{Cd} was incubated with magnesium chloride (Fig. 8D and E). $RelQ_{Cd}$ incubated with ATP and GTP was similarly capable of eradicating the ATP 5′ β phosphate peak in the absence of added metal but did not generate a pGpp 5′ α phosphate peak unless magnesium chloride was present (Fig. 8F to H). $RelQ_{Cd}$ supplemented with magnesium also resulted in separation of the previously overlapping ATP and GTP 5′ α and 5′ γ phosphate peaks, presumably as ATP was hydrolyzed to ADP (Fig. 8F and H). It appears that residual magnesium contamination was sufficient to allow ATP hydrolysis but not pyrophosphotransfer by both of the clostridial synthetases but that the alarmone synthesis observed in the presence of diverse metal cations was in fact dependent upon those metal ion cofactors.

We speculate that tolerance for the clostridial enzymes for a broad range of metal ion cofactor sizes could be an adaptive response to "nutritional immunity," which is the ability of mammalian immune systems to chelate and sequester metal ions that are limiting factors for the growth of foreign pathogens (52). Metal starvation can trigger the stringent response in some bacteria (53, 54). We monitored phiLOV expression under the control of the *rsh* and *relQ* promoters after 1 h of exposure to the metal ion chelator EDTA. Metal depletion by EDTA had no significant effect on *relQ* promoter activity but did increase the activity of P_{rsh} (Fig. 7C). When an equimolar amount of the divalent cations zinc and iron, the best-documented targets of nutritional immunity, was added with the EDTA, the EDTA-induced increase in P_{rsh} activity was abolished. Supplemental zinc and iron did not affect P_{rsh} activity alone (Fig. 7C).

DISCUSSION

The outputs regulated by the SR are highly conserved, as accumulation of the magic spot alarmones causes similar phenotypes in diverse bacteria. However, different mechanisms lead to these convergent results. In this study, we explored the biological role and biochemistry of

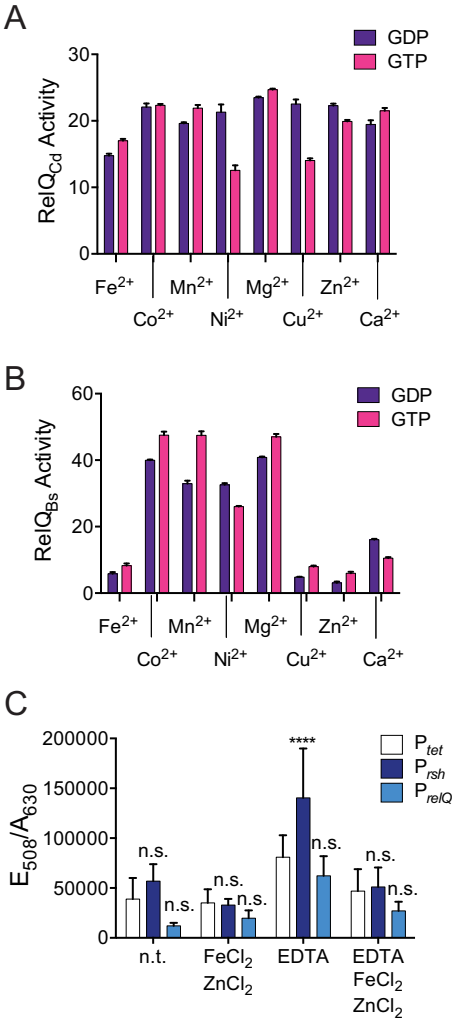

FIG 7 $RelQ_{Cd}$ accommodates a wide range of metal ion cofactors and metal starvation induces *rsh*. (A and B) Pyrophosphotransfer after 60 min from [γ-^{32}P]ATP to a 500 μM concentration of the indicated GXP phosphoacceptor in the presence of a 5.0 mM concentration of the indicated metal ion cofactor by 2.0 μM $RelQ_{Cd}$ (A) or 3.0 μM $RelQ_{Bs}$ (B). Metal ions are arranged in order of increasing ionic size. Shown are the means and standard deviations of three independent samples. (C) PhiLOV fluorescence normalized to cell density after 1 h of exposure to 2 mM EDTA and/or 1 mM $FeCl_2$ and 1 mM $ZnCl_2$. Activity from the P_{rsh} and P_{relQ} promoters was compared to that from the P_{tet} promoter under the same condition by two-way ANOVA. ****, $P < 0.0001$.

the clostridial SAS $RelQ_{Cd}$. Despite the high sequence conservation between $RelQ_{Cd}$ and SAS from other organisms, our results were not entirely as expected.

We have previously demonstrated that stationary-phase onset and exposure to the antibiotics clindamycin and metronidazole stimulate *rsh* transcription in *C. difficile* and

TABLE 3 Ionic radii of divalent metal cofactors[a]

Cation	Effective ionic radius (Å)
Fe^{2+}	0.75
Co^{2+}	0.79
Mn^{2+}	0.81
Ni^{2+}	0.83
Mg^{2+}	0.86
Cu^{2+}	0.87
Zn^{2+}	0.88
Ca^{2+}	1.1

[a]Crystal radii of metal ions in the +2 oxidation state with octahedral coordination. Where two electron configurations are possible, the low spin radius is listed (62, 63).

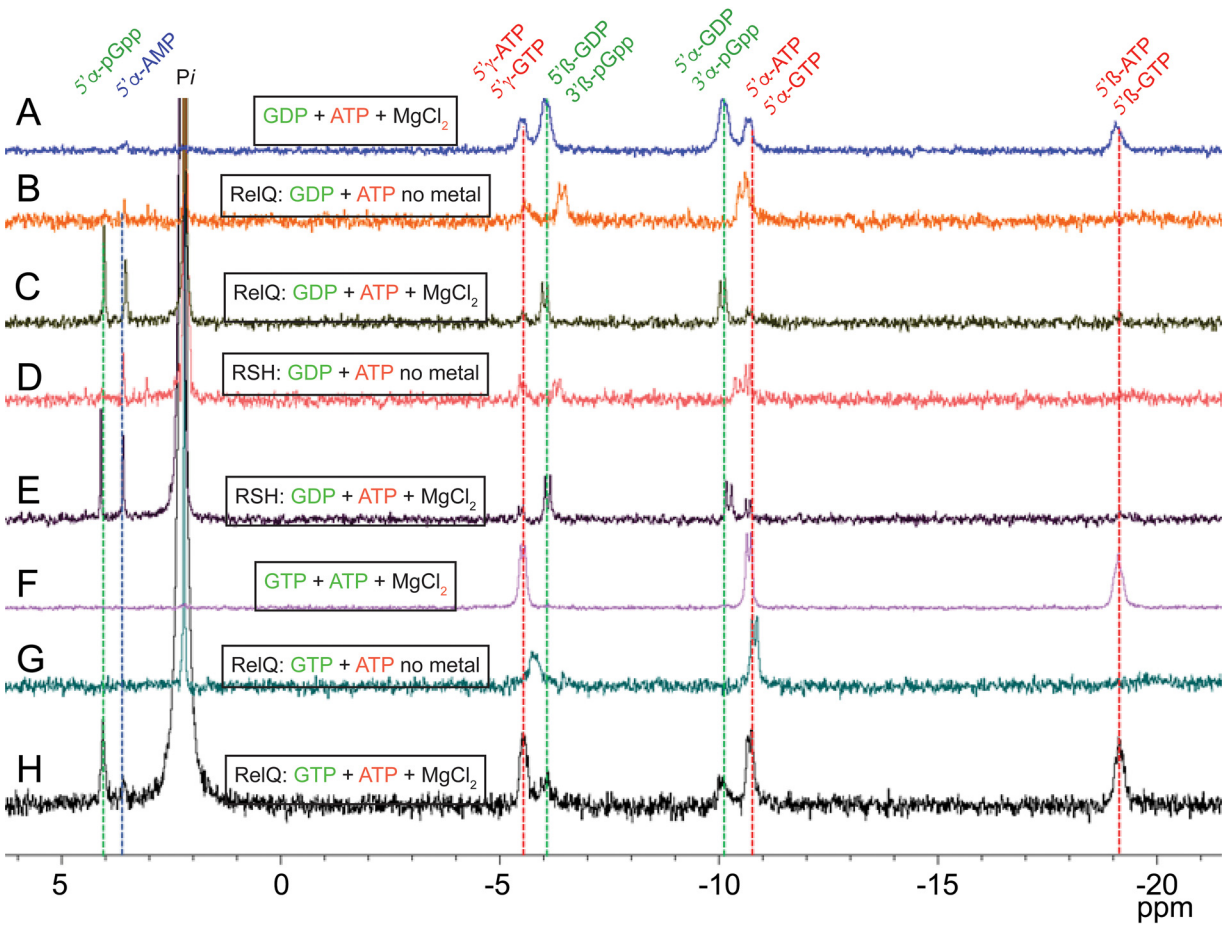

FIG 8 ^{31}P NMR evidence that alarmone synthesis depends on added divalent cations. (A) ATP and GDP incubated with $MgCl_2$. (B) $RelQ_{Cd}$ (2.0 μM) incubated with ATP, GDP, and no residual metal for 40 min. (C) $RelQ_{Cd}$ (2.0 μM) incubated with ATP, GDP, and $MgCl_2$ for 40 min. (D) RSH_{Cd} (3.0 μM) incubated with ATP, GDP, and no residual metal for 60 min. (E) $RelQ_{Cd}$ (2.0 μM) incubated with ATP, GDP, and $MgCl_2$ for 40 min. (F) ATP and GTP incubated with $MgCl_2$. (G) $RelQ_{Cd}$ (2.0 μM) incubated with ATP, GTP, and no residual metal for 40 min. (H) $RelQ_{Cd}$ (2.0 μM) incubated with ATP, GTP, and $MgCl_2$ for 40 min.

that genetic or chemical inhibition of RSH_{Cd} increases antibiotic susceptibility (28). In this study, we confirmed that antibiotic stress stimulates transcription of clostridial stringent response genes in a strain-specific manner; *relQ* responds to fidaxomicin but not vancomycin in R20291 and to vancomycin but not fidaxomicin in 630Δ*erm*. It is tempting to speculate that strain-specific induction of synthetase genes may contribute to observed differences in antibiotic tolerance among *C. difficile* strains, although this will need to be verified by testing in more clinical strains before a conclusion can be drawn. We have previously found that transcription of *rsh* but not *relQ* is induced by stationary-phase onset (28). In this study, we investigated the response of the clinically relevant ribotype 027 strain *C. difficile* R20291 to extracellular stresses representative of those likely to be encountered *in vivo* and found that *rsh* but not *relQ* is upregulated by oxidative and acid stress in this strain. It is possible that RSH is the primary mediator of a stress-induced stringent response in this organism and that the primary role of RelQ is regulation of metabolic homeostasis as has been reported for *B. subtilis* and *E. faecalis* (26, 27). This would be consistent with the greater affinity of $RelQ_{Cd}$ for GTP, which suggests a biological role for $RelQ_{Cd}$ when cytoplasmic GTP is not depleted. Our finding that medium acidification caused by stationary-phase onset in R20291 is sufficient to induce *rsh* transcription in nutrient-rich fresh growth medium suggests that medium acidification due to metabolic activity is one of the signals that regulate the expression of stationary-phase genes in this organism.

Intriguingly, we report that the two clostridial magic spot synthetase enzymes share

characteristics that appear to be unique to *C. difficile*. While some SAS enzymes can directly synthesize pGpp using GMP as a substrate, there is little precedent for a synthetase to produce the triphosphate signal using GDP or GTP as substrates (25, 34, 40–42, 55). There are no known examples of an organism that produces pGpp exclusively. Direct synthesis of pGpp via hydrolysis of GDP or GTP 5′ β phosphate bonds has only been reported as a minor *in vitro* activity of *E. coli* RSH, dependent on the presence of an EKDD motif in the synthetase active site (29). To date, every organism that synthesizes pGpp directly or indirectly also synthesizes ppGpp and pppGpp (25, 34, 40, 55, 56). Utilization of GDP and GTP to exclusively synthesize pGpp by both an RSH and an SAS enzyme has not previously been reported. While it is still possible that RelC synthesizes the longer alarmones despite its nonconserved guanosine binding motif, the dependence of RSH_{Cd} and $RelQ_{Cd}$ on guanosine β phosphate bond hydrolysis indicates that pGpp is a very important, and possibly the only, clostridial alarmone. It is also unusual that $RelQ_{Cd}$ exhibits a higher affinity for GTP than GDP. The only obvious divergence between $RelQ_{Cd}$ and characterized SAS with substrate preferences for GDP is the presence of a glycine in the first position of the GXP binding motif, which is a polar charged residue in all other SAS homologs except *C. glutamicum* RelS, which has a valine at that position and preferentially utilizes GTP (Fig. 1). Previous work in RSH enzymes has posited that an acidic EXDD sequence at the beginning of the guanosine binding motif results in a preference for GDP, while a basic RXKD sequence correlates to a preference for GTP (29). This association does not appear to hold in SAS enzymes, several of which have a basic motif and prefer GDP (Fig. 1). However, it is likely that this position does contribute to the enzyme's ability to utilize GDP or GTP. Future mutational analysis will likely be necessary to determine what residues play a role in guanosine β phosphate bond hydrolysis.

In addition to the unexpected triphosphate alarmone product, the characterized clostridial synthetases share another trait that does not appear to be widespread among RSH or SAS family enzymes: a remarkable ability to utilize structurally diverse divalent cationic cofactors. While few other synthetases have been tested against an expansive panel of divalent cations, cobalt, zinc, copper, nickel, iron, and calcium do not allow synthetase activity by *Mycobacterium tuberculosis* Rel and manganese, nickel, and calcium reduce or abolishes synthetase activity by *M. extorquens* Rel (33, 35). Zinc, but not iron or nickel, stimulates enzymatic activity of crystallized RelP from *S. aureus* (44). There does not appear to be any precedent for the extremely broad range of metals successfully utilized as cofactors by both clostridial synthetases (28). As it appears that metal ion limitation is another stress that induces expression of clostridial *rsh*, it is possible that promiscuous utilization of divalent cations in the enzymes that enact the clostridial stringent response could prevent dependence on any specific cation and provide a survival advantage in metal-limited environments. It is interesting that residual magnesium present after protein purification is sufficient for ATP hydrolysis but not pyrophosphotransfer and that RSH appears to remove a pyrophosphate from ATP while RelQ removes a phosphate. Future structural analyses will be necessary to explore possible mechanistic differences in metal ion usage by the two clostridial enzymes.

Given the role of the SR in antibiotic tolerance and virulence, there is interest in inhibiting it as an antimicrobial strategy (57, 58). However, the ubiquity of this signaling pathway among bacteria means that synthetase inhibitors are likely to exhibit a broad spectrum of action that could diminish the protective effect of the gut microbiota. The discovery that the SR in *C. difficile* is mediated by synthetases whose alarmone product and metal utilization are conserved with each other but different from that of their homologs in other bacterial species raises the possibility that the clostridial enzymes share structural features that distinguish them from synthetases in other organisms. Further characterization of the clostridial synthetase enzymes may provide a foundation for specific, targeted inhibition of the clostridial stringent response, which could

be applied as an adjuvant to antibiotic therapy to diminish *C. difficile* antibiotic survival.

MATERIALS AND METHODS

Cell culture. The bacterial strains and the plasmids used in this study are listed in Table S2. *E. coli* strains were grown in Luria-Bertani (LB) medium at 37°C. *C. difficile* strains were grown anaerobically in brain heart infusion medium supplemented with 5% yeast extract (BHIS). Anaerobic bacterial culture was maintained in a Coy anaerobic chamber (Coy Laboratory Products, Grass lake, MI) with an atmosphere of 85% N_2, 10% CO_2, and 5% H_2 at 37°C. Unless otherwise stated, all the experiments were conducted in *C. difficile* R20291. The pH of the *C. difficile* filtered growth medium was monitored before and after 24 h of incubation using a benchtop pH meter (Mettler-Toledo). To avoid adding spent liquid medium to the fresh samples, cultures used for medium pH experiments were inoculated with single colonies picked from BHIS agar plates. All plastic consumables were equilibrated in the anaerobic chamber for at least 72 h prior to use. Bacterial strains carrying plasmids were maintained using the corresponding antibiotics at the indicated concentrations: 10 μg mL^{-1} of thiamphenicol (Tm10; Alfa Aesar) and 50 μg mL^{-1} of kanamycin (Kan; Bio Basic).

Promoter activity analysis. The *in vivo* promoter activity of the reporter strains was studied as previously described (28). Briefly, saturated starter cultures of *C. difficile* strains containing the phiLOV2.1 reporter plasmid were grown anaerobically at 37°C in BHIS-Tm10 for 12 to 16 h and inoculated 1:50 into fresh BHIS-Tm10 containing indicated treatments (1.70 μg mL^{-1} of vancomycin [VWR], 0.67 μg mL^{-1} of fidaxomicin [Cayman Chemical], 1.0 mM diamide [MP Biomedicals], 4.0 μM copper sulfate [Fisher Scientific]). For metal starvation, log-phase cells (optical density at 600 nm [OD_{600}], 0.50 to 0.70) were exposed to 1 mM $FeCl_2$ (Acros Organics) and 1 mM $ZnCl_2$ (Acros Organics) or 2 mM freshly suspended EDTA (Fisher Scientific) with 1 mM $FeCl_2$ and 1 mM $ZnCl_2$, and grown for 1 h at 37°C. To monitor temperature-induced promoter activity, log-phase cells (OD_{600}, 0.50 to 0.70) of each of the strains were divided into halves and incubated in parallel at 37°C and 41°C for 30 min. pH-induced promoter activity was measured by inoculating exponentially growing cells 1:50 into BHIS-Tm10 containing 0.1 M potassium phosphate buffer at pH 6.0, 7.0, 8.0, or 9.0. OD_{600} was recorded for each sample upon collection. To minimize discrepancies in fluorescent signal from cellular autofluorescence, cell numbers in each sample were equalized on collection. Each sample was collected at a volume that would give a cell count equivalent to 3 mL of the culture with the lowest OD_{600}. After collection, cells were pelleted anaerobically in a microcentrifuge and suspended in 400 μL of anaerobic 1× phosphate-buffered saline (PBS). Duplicate 200-μL samples were aliquoted into a clear-bottomed black 96-welled microplate (Thermo Fisher Scientific) and were removed from the anaerobic chamber to measure sample fluorescence intensity. Sample fluorescence using 440-/30-nm excitation and 508-/20/nm emission filters and sample OD_{630} were measured on a BrandTek plate reader. The instrumental parameters for all fluorescence measurements included a sensitivity limit of 65. Measurements were blanked against 1× PBS and were reported as E_{508}/A_{630}. All measurements were performed on at least six biologically independent samples. Statistical analysis was performed using Prism (GraphPad).

Cloning of $RelQ_{cd}$. The *relQ* gene (CDR20291_0350) was amplified from *C. difficile* R20291 genomic DNA using gene specific primers (5′relQ_NdeI and 3′relQ_XhoI). The *relQ* amplicon was ligated into pET24a expression vector at the NdeI-XhoI restriction sites and upstream of the vector-derived 6×His tag to generate pET24a::relQ plasmid. The plasmid was transformed into *E. coli* BL21 (New England BioLabs [NEB]) and confirmed by PCR using *relQ* gene-specific primers (relQ_a_F and relQ_a_R) (Table S2).

***In vivo* overexpression of RelQ.** Growth curve assays following the induction of *C. difficile relQ* in *E. coli* BL21 cells carrying pMMBneo::relQ were performed in 96-well microtiter plates (Brand Plates) using a BioTek Synergy plate reader. Exponential-phase cultures of *E. coli* were inoculated in LB medium in the presence or absence of 0.5 mM isopropyl-β-D-thiogalactopyranoside (IPTG) inducer. The plate was incubated at 37°C with shaking for a total of 16 h while monitoring cell growth every 30 min.

$RelQ_{cd}$ expression and purification. Saturated starter cultures of *E. coli* BL21 cells containing pET24a-$RelQ_{cd}$-His plasmid were grown overnight in LB medium with 50 μg mL^{-1} of kanamycin in a shaking incubator at 250 rpm and 37°C. Cultures were diluted 1:20 into LB medium with 50 μg mL^{-1} of kanamycin and grown at 37°C with shaking until the optical density at 600 nm reached 0.5 to 0.6. Once cells reached the desired OD_{600}, they were allowed to stand at room temperature for 10 min and induced with 0.5 mM IPTG for 3 h at 30°C for protein expression. Cells were centrifuged at a relative centrifugal force (rcf) of 4,030 using a Beckman coulter JA12 rotor for 30 min at 4°C, and pellets were frozen at −20°C. Cells were lysed using lysis buffer (50 mM Tris-HCl [pH 8.0], 500 mM NaCl, 5 mM $MgCl_2$, 10 mM imidazole, 3 mM β-mercaptoethanol (BME), and 100 mM phenylmethylsulfonyl fluoride [PMSF]) via sonication. The cells were burst for 10 s at 40% amplitude with 30-s pause for 8 cycles, followed by centrifugation at 13,680 × *g* for 15 min at 4°C in a benchtop Scilogex centrifuge. The soluble protein fraction was collected as supernatant and subjected for purification using HisPur nickel-nitrilotriacetic acid (Ni-NTA) resin affinity chromatography (Thermo Fisher Scientific). Briefly, the supernatant was mixed with equilibrating buffer (same as lysis buffer) in 1:1 ratio and subjected to a 1.0-mL Ni-NTA resin column equilibrated with the equilibrating buffer. Initially the column was washed with five column volumes of the lysis buffer and then further washed and eluted using a gradient of imidazole: 30 mM, 50 mM, and 75 mM concentrations of imidazole were used for column washing, while the protein was eluted using 150 mM and 300 mM imidazole in two fractions. Purified protein was subsequently dialyzed overnight at 4°C in a buffer consisting of 30 mM Tris (pH 8.0), 300 mM NaCl, 5 mM $MgCl_2$, 5 mM BME, and 20% glycerol. Protein concentration was determined spectroscopically, measuring A_{280} using a BioDrop

instrument. A molar extinction coefficient of 36,455 $M^{-1}cm^{-1}$ as determined by ExPASy (59) for $RelQ_{Cd}$ was used to estimate the concentration.

Expression and purification of the control synthetase. *E. coli* BL21 cells carrying pET28 bearing the *Bacillus subtilis* SAS1/RelQ gene were generously provided by Mingxu Fang, University of California, San Diego, and Carl E. Bauer, Indiana University, Bloomington. *Bacillus subtilis* RelQ was expressed and purified using a protocol developed by Mingxu Fang as previously published (43). Briefly, *E. coli* BL21 cells bearing pET28a::$RelQ_{Bs}$ were grown in LB media containing 50 μg mL^{-1} of kanamycin at 37°C with shaking until the OD_{600} reached 0.4. Protein expression was induced overnight at 16°C by the addition of 200 μM IPTG. Cell pellet was collected by centrifugation at 4°C and resuspended in StrepTactin buffer containing 50 mM Tris (pH 8.9), 1 M NaCl, and 20% glycerol along with 2 mM PMSF. The cells were sonicated with a 10-s burst and 30-s pause cycle at 40% amplitude for 8 cycles, followed by centrifugation to collect the clarified lysate. The protein was purified by using StrepTactin resin column (IBA Life sciences) following the manufacturer's instructions.

***In vitro* measurement of synthetase activity.** (pp)pGpp synthesis was carried in a reaction volume of 10.0 μL as described previously (28, 60) with a fixed concentration of $RelQ_{Cd}$ or $RelQ_{Bs}$. The reaction mixture consisted of a buffer containing 10 mM Tris-HCl (pH 7.5), 5 mM ammonium acetate, 2 mM KCl, 0.2 mM dithiothreitol (DTT), 0.15 mM ATP, 5 mM $MgCl_2$, 1.0 μCi of [γ-^{32}P]ATP (PerkinElmer), and desired concentrations of AMP (Acros Organics)/ADP/ATP (Bio Basic)/GMP (BioPlus Chemicals)/GDP/GTP (Bio Basic) phosphoacceptor. Where indicated, the pH of the reaction was adjusted with HCl or NaOH. Where indicated, $MgCl_2$ was replaced with 5 mM metal salts in the +2 oxidation state ($MnCl_2$, $CoCl_2$, $CuCl_2$, $ZnCl_2$, $NiBr_2$, $CaCl_2$, and $FeSO_4$). The reactions occurred at 37°C and were stopped by spotting 2.0 μL of each sample onto polyethyleneimine (PEI)-cellulose thin-layer chromatography (TLC) plates, allowing the spots to dry. Unless otherwise indicated, reactions were run for 60 min before quenching. The plates were subsequently developed in 1.5 M KH_2PO_4 (pH 3.64 $\pm$ 0.03) and autoradiographed using a Storm 860 phosphorimager (GE Healthcare Life Sciences). pGpp signal was quantitated using ImageJ software to measure signal in each spot on the TLC plate and correct for background signal as previously described (60, 61). RelQ activity was expressed as the percentage of [γ-^{32}P]ATP substrate converted into product at each time point as described previously (60). Michaelis-Menten assays were performed by running the reactions for 5 min at the indicated concentration of GDP or GTP. Data shown are the means and standard deviations from two experiments. The line of best fit for the Michaelis-Menten equation was calculated using nonlinear regression with least-squares fit and the equation $y = (V_{max} \times X)/(K_M + X)$, where X represents the GXP substrate concentration and y represents the initial reaction velocity, and graphed with Prism (GraphPad).

Hydrolase contaminant check. $RelQ_{Bs}$ synthesis reaction mixtures containing either GDP or GTP as substrates were conducted for 60 min at 37°C as described above. $RelQ_{Cd}$ was added to each reaction at a final concentration of 2.0 μM and incubated for an additional 60 min. At 0, 30, and 60 min after $RelQ_{Cd}$ addition, 2.0 μL of each reaction mixture was spotted into the PEI-TLC plates for development as described above.

GXP phosphatase activity. Guanosine nucleotide hydrolysis was assessed through synthetase assays performed as described above using guanosine 5′-β-thio-diphosphate trilithium salt (GDPβS) as the only nucleotide phosphoacceptor (Millipore Sigma). The reactions were caried out for 60 min at 37°C, and the spots were autoradiographed as reported above.

^{31}P NMR spectroscopy. The structural properties of the newly synthesized product were also evaluated by phosphorus NMR. Synthesis reactions were carried out with clostridial synthetases as mentioned above for 40 min at 37°C, and the reaction mixtures were subjected to acquire phosphorus NMR spectra. For "no metal" experiments, reactions were performed in 10 mM Tris-HCl (pH 7.5) containing 5 mM ammonium acetate, 2 mM KCl, 0.2 mM DTT, and no additional divalent cations. In addition, phosphorus NMR spectra of the standard nucleotides (ATP, GTP, GDP, GMP, and AMP) solutions in the reaction buffer containing 5 mM $MgCl_2$ were also acquired for signal comparison and assignments. D_2O at 15% was added into each of the samples to enable locking of the magnetic field in the NMR spectrometer. NMR spectra were indirectly referenced to 85% external phosphoric acid. ^{31}P NMR recordings with proton decoupling were performed using a 400-MHz Bruker Avance III HD NMR spectrometer at 162 MHz (^{31}P) equipped with a 5-mm PABBO BB/19F-1H/D Z-GRD Z108618/0798 probe. A total of 14,000 scans for each sample at 303 K were performed to acquire NMR spectra. All the measurements were carried out using pulse sequences supplied by the spectrometer manufacturer (Bruker TopSpin 3.2).

Isothermal calorimetry (ITC). ITC200 microcalorimeter (Malvern) was employed for the analysis of the binding affinity of $RelQ_{Cd}$ toward GXP as described previously (28). Briefly, a total volume of 300 μL of reaction buffer containing 0.006 mM protein was added into the cell component and 40 μL of 0.06 mM GXP was filled into the syringe, from which a total of 38 injections were made for the analysis at 37°C. Both the protein and ligands were prepared in the same buffer containing 10 mM Tris-Cl, 5 mM ammonium acetate (AmAce), 5 mM $MgCl_2$, 0.2 mM DTT, 0.12 mM ATP, and 2 mM KCl. The data obtained were processed in Origin software using a single-binding-site model. The heats of dilution acquired through the titration of ligand into the reference solution were subtracted from the binding curves during peak integration and the calculation of thermodynamic parameters. Two independent samples were measured.

Data availability. The data that support the findings of this study are available from the corresponding author upon reasonable request.

SUPPLEMENTAL MATERIAL

Supplemental material is available online only.

SUPPLEMENTAL FILE 1, PDF file, 0.4 MB.

ACKNOWLEDGMENTS

We thank Carl Bauer of Indiana University, Bloomington, for the $RelQ_{Bs}$ expression vector and Mingxu Fang of University of California, San Diego, for very helpful troubleshooting discussions during enzyme purification. We thank Alvin Holder of Old Dominion University for use of the ITC instrument and helpful discussion of metal cofactors and Michael Celestine of Old Dominion University for assistance with ITC. We thank Steven Pascal of Old Dominion University for very helpful discussion of NMR data.

This work was funded by the National Institutes of Health (1K22AI118929-01) and by startup funds from Old Dominion University. Estevan J. Coronado and Marrett M. Gilfus were supported by NSF REU CHE-1659476.

We declare no financial conflict of interest.

REFERENCES

1. Guh AY, Mu Y, Winston LG, Johnston H, Olson D, Farley MM, Wilson LE, Holzbauer SM, Phipps EC, Dumyati GK, Beldavs ZG, Kainer MA, Karlsson M, Gerding DN, McDonald LC, Emerging Infections Program Clostridioides difficile Infection Working G. 2020. Trends in U.S. burden of *Clostridioides difficile* infection and outcomes. N Engl J Med 382:1320–1330. https://doi.org/10.1056/NEJMoa1910215.
2. Deakin LJ, Clare S, Fagan RP, Dawson LF, Pickard DJ, West MR, Wren BW, Fairweather NF, Dougan G, Lawley TD. 2012. The Clostridium difficile spo0A gene is a persistence and transmission factor. Infect Immun 80:2704–2711. https://doi.org/10.1128/IAI.00147-12.
3. Gil F, Lagos-Moraga S, Calderón-Romero P, Pizarro-Guajardo M, Paredes-Sabja D. 2017. Updates on *Clostridium difficile* spore biology. Anaerobe 45:3–9. https://doi.org/10.1016/j.anaerobe.2017.02.018.
4. Eze P, Balsells E, Kyaw MH, Nair H. 2017. Risk factors for Clostridium difficile infections—an overview of the evidence base and challenges in data synthesis. J Glob Health 7:e010417. https://doi.org/10.7189/jogh.07.010417.
5. Britton RA, Young VB. 2014. Role of the intestinal microbiota in resistance to colonization by Clostridium difficile. Gastroenterology 146:1547–1553. https://doi.org/10.1053/j.gastro.2014.01.059.
6. Wetzel D, McBride SM. 2020. The impact of pH on Clostridioides difficile sporulation and physiology. Appl Environ Microbiol 86:e02706-19. https://doi.org/10.1128/AEM.02706-19.
7. Buffie CG, Bucci V, Stein RR, McKenney PT, Ling L, Gobourne A, No D, Liu H, Kinnebrew M, Viale A, Littmann E, van den Brink MR, Jenq RR, Taur Y, Sander C, Cross JR, Toussaint NC, Xavier JB, Pamer EG. 2015. Precision microbiome reconstitution restores bile acid mediated resistance to *Clostridium difficile*. Nature 517:205–208. https://doi.org/10.1038/nature13828.
8. von Schwartzenberg RJ, Bisanz JE, Lyalina S, Spanogiannopoulos P, Ang QY, Cai J, Dickmann S, Friedrich M, Liu SY, Collins SL, Ingebrigtsen D, Miller S, Turnbaugh JA, Patterson AD, Pollard KS, Mai K, Spranger J, Turnbaugh PJ. 2021. Caloric restriction disrupts the microbiota and colonization resistance. Nature 595:272–277. https://doi.org/10.1038/s41586-021-03663-4.
9. Evans SS, Repasky EA, Fisher DT. 2015. Fever and the thermal regulation of immunity: the immune system feels the heat. Nat Rev Immunol 15:335–349. https://doi.org/10.1038/nri3843.
10. Joo HS, Fu CI, Otto M. 2016. Bacterial strategies of resistance to antimicrobial peptides. Philos Trans R Soc Lond B Biol Sci 371:20150292. https://doi.org/10.1098/rstb.2015.0292.
11. Fang FC, Frawley ER, Tapscott T, Vázquez-Torres A. 2016. Bacterial stress responses during host infection. Cell Host Microbe 20:133–143. https://doi.org/10.1016/j.chom.2016.07.009.
12. Trastoy R, Manso T, Fernández-García L, Blasco L, Ambroa A, Pérez Del Molino ML, Bou G, García-Contreras R, Wood TK, Tomás M. 2018. Mechanisms of bacterial tolerance and persistence in the gastrointestinal and respiratory environments. Clin Microbiol Rev 31:e00023-18. https://doi.org/10.1128/CMR.00023-18.
13. Girinathan BP, Braun SE, Govind R. 2014. Clostridium difficile glutamate dehydrogenase is a secreted enzyme that confers resistance to H2O2. Microbiology (Reading) 160:47–55. https://doi.org/10.1099/mic.0.071365-0.
14. Irving SE, Corrigan RM. 2018. Triggering the stringent response: signals responsible for activating (p)ppGpp synthesis in bacteria. Microbiology (Reading) 164:268–276. https://doi.org/10.1099/mic.0.000621.
15. Dalebroux ZD, Svensson SL, Gaynor EC, Swanson MS. 2010. ppGpp conjures bacterial virulence. Microbiol Mol Biol Rev 74:171–199. https://doi.org/10.1128/MMBR.00046-09.
16. Irving SE, Choudhury NR, Corrigan RM. 2021. The stringent response and physiological roles of (pp)pGpp in bacteria. Nat Rev Microbiol 19:256–271. https://doi.org/10.1038/s41579-020-00470-y.
17. Hauryliuk V, Atkinson GC, Murakami KS, Tenson T, Gerdes K. 2015. Recent functional insights into the role of (p)ppGpp in bacterial physiology. Nat Rev Microbiol 13:298–309. https://doi.org/10.1038/nrmicro3448.
18. Atkinson GC, Tenson T, Hauryliuk V. 2011. The RelA/SpoT homolog (RSH) superfamily: distribution and functional evolution of ppGpp synthetases and hydrolases across the tree of life. PLoS One 6:e23479. https://doi.org/10.1371/journal.pone.0023479.
19. Ma Z, King K, Alqahtani M, Worden M, Muthuraman P, Cioffi CL, Bakshi CS, Malik M. 2019. Stringent response governs the oxidative stress resistance and virulence of Francisella tularensis. PLoS One 14:e0224094. https://doi.org/10.1371/journal.pone.0224094.
20. Schäfer H, Beckert B, Frese CK, Steinchen W, Nuss AM, Beckstette M, Hantke I, Driller K, Sudzinová P, Krásný L, Kaever V, Dersch P, Bange G, Wilson DN, Turgay K. 2020. The alarmones (p)ppGpp are part of the heat shock response of Bacillus subtilis. PLoS Genet 16:e1008275. https://doi.org/10.1371/journal.pgen.1008275.
21. Ronneau S, Hallez R. 2019. Make and break the alarmone: regulation of (p)ppGpp synthetase/hydrolase enzymes in bacteria. FEMS Microbiol Rev 43:389–400. https://doi.org/10.1093/femsre/fuz009.
22. Takada H, Roghanian M, Caballero-Montes J, Van Nerom K, Jimmy S, Kudrin P, Trebini F, Murayama R, Akanuma G, Garcia-Pino A, Hauryliuk V. 2021. Ribosome association primes the stringent factor Rel for tRNA-dependent locking in the A-site and activation of (p)ppGpp synthesis. Nucleic Acids Res 49:444–457. https://doi.org/10.1093/nar/gkaa1187.
23. Brown A, Fernández IS, Gordiyenko Y, Ramakrishnan V. 2016. Ribosome-dependent activation of stringent control. Nature 534:277–280. https://doi.org/10.1038/nature17675.
24. Steinchen W, Vogt MS, Altegoer F, Giammarinaro PI, Horvatek P, Wolz C, Bange G. 2018. Structural and mechanistic divergence of the small (p)ppGpp synthetases RelP and RelQ. Sci Rep 8:2195. https://doi.org/10.1038/s41598-018-20634-4.
25. Gaca AO, Colomer-Winter C, Lemos JA. 2015. Many means to a common end: the intricacies of (p)ppGpp metabolism and its control of bacterial homeostasis. J Bacteriol 197:1146–1156. https://doi.org/10.1128/JB.02577-14.
26. Gaca AO, Kajfasz JK, Miller JH, Liu K, Wang JD, Abranches J, Lemos JA. 2013. Basal levels of (p)ppGpp in Enterococcus faecalis: the magic beyond the stringent response. mBio 4:e00646-13. https://doi.org/10.1128/mBio.00646-13.
27. Kriel A, Brinsmade SR, Tse JL, Tehranchi AK, Bittner AN, Sonenshein AL, Wang JD. 2014. GTP dysregulation in Bacillus subtilis cells lacking (p)ppGpp results in phenotypic amino acid auxotrophy and failure to adapt to nutrient downshift and regulate biosynthesis genes. J Bacteriol 196:189–201. https://doi.org/10.1128/JB.00918-13.
28. Pokhrel A, Poudel A, Castro KB, Celestine MJ, Oludiran A, Rinehold AJ, Resek AM, Mhanna MA, Purcell EB. 2020. The (p)ppGpp synthetase RSH mediates stationary-phase onset and antibiotic stress survival in Clostridioides difficile. J Bacteriol 202:e00377-20. https://doi.org/10.1128/JB.00377-20.

29. Sajish M, Kalayil S, Verma SK, Nandicoori VK, Prakash B. 2009. The significance of EXDD and RXKD motif conservation in Rel proteins. J Biol Chem 284:9115–9123. https://doi.org/10.1074/jbc.M807187200.
30. Sajish M, Tiwari D, Rananaware D, Nandicoori VK, Prakash B. 2007. A charge reversal differentiates (p)ppGpp synthesis by monofunctional and bifunctional Rel proteins. J Biol Chem 282:34977–34983. https://doi.org/10.1074/jbc.M704828200.
31. Steinchen W, Schuhmacher JS, Altegoer F, Fage CD, Srinivasan V, Linne U, Marahiel MA, Bange G. 2015. Catalytic mechanism and allosteric regulation of an oligomeric (p)ppGpp synthetase by an alarmone. Proc Natl Acad Sci U S A 112:13348–13353. https://doi.org/10.1073/pnas.1505271112.
32. Mechold U, Murphy H, Brown L, Cashel M. 2002. Intramolecular regulation of the opposing (p)ppGpp catalytic activities of RelSeq, the Rel/Spo enzyme from Streptococcus equisimilis. J Bacteriol 184:2878–2888. https://doi.org/10.1128/JB.184.11.2878-2888.2002.
33. Avarbock D, Avarbock A, Rubin H. 2000. Differential regulation of opposing RelMtb activities by the aminoacylation state of a tRNA·ribosome·mRNA·RelMtb complex. Biochemistry 39:11640–11648. https://doi.org/10.1021/bi001256k.
34. Fung DK, Yang J, Stevenson DM, Amador-Noguez D, Wang JD. 2020. Small alarmone synthetase SasA expression leads to concomitant accumulation of pGpp, ppApp, and AppppA in Bacillus subtilis. Front Microbiol 11:2083. https://doi.org/10.3389/fmicb.2020.02083.
35. Sobala M, Bruhn-Olszewska B, Cashel M, Potrykus K. 2019. Methylobacterium extorquens RSH enzyme synthesizes (p)ppGpp and pppApp in vitro and in vivo, and leads to discovery of pppApp synthesis in Escherichia coli. Front Microbiol 10:859. https://doi.org/10.3389/fmicb.2019.00859.
36. Nanamiya H, Kasai K, Nozawa A, Yun C-S, Narisawa T, Murakami K, Natori Y, Kawamura F, Tozawa Y. 2008. Identification and functional analysis of novel (p)ppGpp synthetase genes in Bacillus subtilis. Mol Microbiol 67:291–304. https://doi.org/10.1111/j.1365-2958.2007.06018.x.
37. Geiger T, Kastle B, Gratani FL, Goerke C, Wolz C. 2014. Two small (p)ppGpp synthases in Staphylococcus aureus mediate tolerance against cell envelope stress conditions. J Bacteriol 196:894–902. https://doi.org/10.1128/JB.01201-13.
38. Petchiappan A, Naik SY, Chatterji D. 2020. RelZ-mediated stress response in Mycobacterium smegmatis: pGpp synthesis and its regulation. J Bacteriol 202:e00444-19. https://doi.org/10.1128/JB.00444-19.
39. Ruwe M, Ruckert C, Kalinowski J, Persicke M. 2018. Functional characterization of a small alarmone hydrolase in Corynebacterium glutamicum. Front Microbiol 9:916. https://doi.org/10.3389/fmicb.2018.00916.
40. Yang J, Anderson BW, Turdiev A, Turdiev H, Stevenson DM, Amador-Noguez D, Lee VT, Wang JD. 2020. The nucleotide pGpp acts as a third alarmone in Bacillus, with functions distinct from those of (p)ppGpp. Nat Commun 11:5388. https://doi.org/10.1038/s41467-020-19166-1.
41. Zhang Y, Zborníková E, Rejman D, Gerdes K. 2018. Novel (p)ppGpp binding and metabolizing proteins of Escherichia coli. mBio 9:e02188-17. https://doi.org/10.1128/mBio.02188-17.
42. Ooga T, Ohashi Y, Kuramitsu S, Koyama Y, Tomita M, Soga T, Masui R. 2009. Degradation of ppGpp by Nudix pyrophosphatase modulates the transition of growth phase in the bacterium Thermus thermophilus. J Biol Chem 284:15549–15556. https://doi.org/10.1074/jbc.M900582200.
43. Pokhrel A. 2021. Evaluating the role of the stringent response mechanism in Clostridioides difficile survival and pathogenesis. PhD dissertation. Old Dominion University, Norfolk, VA. https://doi.org/10.25777/05ee-2b17.
44. Manav MC, Beljantseva J, Bojer MS, Tenson T, Ingmer H, Hauryliuk V, Brodersen DE. 2018. Structural basis for (p)ppGpp synthesis by the Staphylococcus aureus small alarmone synthetase RelP. J Biol Chem 293:3254–3264. https://doi.org/10.1074/jbc.RA117.001374.
45. Singh T, Bedi P, Bumrah K, Singh J, Rai M, Seelam S. 2019. Updates in treatment of recurrent Clostridium difficile infection. J Clin Med Res 11:465–471. https://doi.org/10.14740/jocmr3854.
46. Stevens VW, Khader K, Echevarria K, Nelson RE, Zhang Y, Jones M, Timbrook TT, Samore MH, Rubin MA. 2020. Use of oral vancomycin for Clostridioides difficile infection and the risk of vancomycin-resistant enterococci. Clin Infect Dis 71:645–651. https://doi.org/10.1093/cid/ciz871.
47. Oludiran A, Courson DS, Stuart MD, Radwan AR, Poutsma JC, Cotten ML, Purcell EB. 2019. How oxygen availability affects the antimicrobial efficacy of host defense peptides: lessons learned from studying the copper-binding peptides piscidins 1 and 3. Int J Mol Sci 20:5289. https://doi.org/10.3390/ijms20215289.
48. Rocha ER, Tzianabos AO, Smith CJ. 2007. Thioredoxin reductase is essential for thiol/disulfide redox control and oxidative stress survival of the anaerobe Bacteroides fragilis. J Bacteriol 189:8015–8023. https://doi.org/10.1128/JB.00714-07.
49. Beljantseva J, Kudrin P, Andresen L, Shingler V, Atkinson GC, Tenson T, Hauryliuk V. 2017. Negative allosteric regulation of Enterococcus faecalis small alarmone synthetase RelQ by single-stranded RNA. Proc Natl Acad Sci U S A 114:3726–3731. https://doi.org/10.1073/pnas.1617868114.
50. Nardi-Schreiber A, Sapir G, Gamliel A, Kakhlon O, Sosna J, Gomori JM, Meiner V, Lossos A, Katz-Brull R. 2017. Defective ATP breakdown activity related to an ENTPD1 gene mutation demonstrated using (31)P NMR spectroscopy. Chem Commun (Camb) 53:9121–9124. https://doi.org/10.1039/c7cc00426e.
51. Spoerner M, Karl M, Lopes P, Hoering M, Loeffel K, Nuehs A, Adelsberger J, Kremer W, Kalbitzer HR. 2017. High pressure (31)P NMR spectroscopy on guanine nucleotides. J Biomol NMR 67:1–13. https://doi.org/10.1007/s10858-016-0079-0.
52. Becker KW, Skaar EP. 2014. Metal limitation and toxicity at the interface between host and pathogen. FEMS Microbiol Rev 38:1235–1249. https://doi.org/10.1111/1574-6976.12087.
53. Miethke M, Westers H, Blom E-J, Kuipers OP, Marahiel MA. 2006. Iron starvation triggers the stringent response and induces amino acid biosynthesis for bacillibactin production in Bacillus subtilis. J Bacteriol 188:8655–8657. https://doi.org/10.1128/JB.01049-06.
54. Colomer-Winter C, Gaca AO, Lemos JA. 2017. Association of metal homeostasis and (p)ppGpp regulation in the pathophysiology of Enterococcus faecalis. Infect Immun 85:e00260-17. https://doi.org/10.1128/IAI.00260-17.
55. Tagami K, Nanamiya H, Kazo Y, Maehashi M, Suzuki S, Namba E, Hoshiya M, Hanai R, Tozawa Y, Morimoto T, Ogasawara N, Kageyama Y, Ara K, Ozaki K, Yoshida M, Kuroiwa H, Kuroiwa T, Ohashi Y, Kawamura F. 2012. Expression of a small (p)ppGpp synthetase, YwaC, in the (p)ppGpp0 mutant of Bacillus subtilis triggers YvyD-dependent dimerization of ribosome. Microbiologyopen 1:115–134. https://doi.org/10.1002/mbo3.16.
56. Yang N, Xie S, Tang NY, Choi MY, Wang Y, Watt RM. 2019. The Ps and Qs of alarmone synthesis in Staphylococcus aureus. PLoS One 14:e0213630. https://doi.org/10.1371/journal.pone.0213630.
57. Syal K, Flentie K, Bhardwaj N, Maiti K, Jayaraman N, Stallings CL, Chatterji D. 2017. Synthetic (p)ppGpp analogue is an inhibitor of stringent response in mycobacteria. Antimicrob Agents Chemother 61:e00443-17. https://doi.org/10.1128/AAC.00443-17.
58. Wexselblatt E, Oppenheimer-Shaanan Y, Kaspy I, London N, Schueler-Furman O, Yavin E, Glaser G, Katzhendler J, Ben-Yehuda S. 2012. Relacin, a novel antibacterial agent targeting the stringent response. PLoS Pathog 8:e1002925. https://doi.org/10.1371/journal.ppat.1002925.
59. Gasteiger E, Gattiker A, Hoogland C, Ivanyi I, Appel RD, Bairoch A. 2003. ExPASy: the proteomics server for in-depth protein knowledge and analysis. Nucleic Acids Res 31:3784–3788. https://doi.org/10.1093/nar/gkg563.
60. Pokhrel A, Poudel A, Purcell EB. 2018. A purification and in vitro activity assay for a (p)ppGpp synthetase from Clostridium difficile. J Vis Exp 2018(141):e58547. https://doi.org/10.3791/58547.
61. Schneider CA, Rasband WS, Eliceiri KW. 2012. NIH Image to ImageJ: 25 years of image analysis. Nat Methods 9:671–675. https://doi.org/10.1038/nmeth.2089.
62. Shannon RD. 1976. Revised effective ionic radii and systematic studies of interatomic distances in halides and chalcogenides. Acta Crystallogr A 32:751–767. https://doi.org/10.1107/S0567739476001551.
63. Schmidt SB, Husted S. 2019. The biochemical properties of manganese in plants. Plants (Basel) 8(10):381. https://doi.org/10.3390/plants8100381.